Refractive Hard X-ray Vortex Phase Plates

FRANK SEIBOTH[1,2,*], MAIK KAHNT[1,3], MIKHAIL LYUBOMIRSKIY[1], MARTIN SEYRICH[1,3], FELIX WITTWER[1,3], TOBIAS ULLSPERGER[4], STEFAN NOLTE[4], DARREN BATEY[5], CHRISTOPH RAU[5], AND CHRISTIAN G. SCHROER[1,3]

[1] *Deutsches Elektronen-Synchrotron DESY, Notkestraße 85, 22607 Hamburg, Germany*
[2] *Linac Coherent Light Source, SLAC National Accelerator Laboratory, 2575 Sand Hill Road, Menlo Park, CA 94025, USA*
[3] *Department Physik, Universität Hamburg, Luruper Chaussee 149, 22761 Hamburg, Germany*
[4] *Institute of Applied Physics, Friedrich-Schiller-Universität Jena, Albert-Einstein-Straße 15, 07745 Jena, Germany*
[5] *Diamond Light Source Ltd., Diamond House, Harwell Science and Innovation Campus, Didcot, Oxfordshire OX11 0DE, UK*
[*] *Corresponding author: frank.seiboth@desy.de*

Compiled June 20, 2019

In this letter we report on the creation of hard X-ray beams carrying orbital angular momentum of topological charge $-\hbar$ and $-3\hbar$ at a photon energy of 8.2 keV via spiral phase plates made out of fused silica by ultrashort-pulsed laser ablation. The phase plates feature a smooth phase ramp with 0.5 µm nominal step height and a surface roughness of 0.5 µm. The measured vortex beams show sub-micrometer sized donut rings and agree well with numerical modeling. Fused silica phase plates are potentially suited to manipulate the electromagnetic field in highly intense X-ray beams at X-ray free-electron laser sources. © 2019 Optical Society of America

OCIS codes: (340.0340) X-ray optics; (120.0120) Instrumentation, measurement, and metrology; (220.0220) Optical design and fabrication; (260.6042) Singular optics.

http://dx.doi.org/10.1364/ao.XX.XXXXXX

Advances in controlling the wavefront, polarization, and orbital angular momentum (OAM) of wavefields in the visible have led to the generation of three-dimensional, structured optical fields [1]. In particular, photons in singular electromagnetic beams with a helically-shaped phase distribution that spirals around its propagation axis and carry an OAM of topological charge $l\hbar$, also known as vortex or twisted beam, have led to a number of new applications. Optical manipulation by traps and tweezers [2, 3], multiplexing of information [4], interferometric imaging [5], or super-resolution microscopy [6] are only a few of them. The generation of vortex beams in the hard X-ray regime has been explored in the past by conventionally manipulating the beam via stepped refractive phase plates [7] out of polyimide or as binary, diffractive structures by gold electroplating [8] or ion beam milling [9]. While a coarsely stepped phase plate can lead to artifacts and an imperfect beam shape, especially for higher topological charges, the binary structures made of heavy elements are often not suited for peak intensities at X-ray free-electron laser (XFEL) sources [10, 11]. More recently, the direct generation of X-ray beams carrying OAM has been reported as higher harmonics in a helical undulator [12, 13], as fundamental radiation through laser-manipulated electron beams in a planar undulator [14], or via echo-enabled harmonic generation [15]. These techniques enable significantly more intense vortex beams, however, they require sophisticated instrumentation and fast switching between topological charges might be difficult.

Here, we present finely stepped vortex plates made by ultrashort-pulse laser ablation out of fused silica, as shown in Fig. 1. The height ramp in Fig. 1a shows almost no visible steps. For the steeper gradients in Fig. 1b steps become slightly visible. The structures were fabricated using a Trumpf TruMicro5050 picosecond laser, operating at a wavelength of 1030 nm with a pulse duration of 8 ps and pulse energy of 0.5 µJ. The laser pulses were focused on the backside of the sample with a numerical aperture (NA) 0.35 objective, resulting in a spot size of roughly 2 µm. Individual layers with a nominal height of 0.5 µm were sequentially ablated from the fused silica substrate that has a thickness of 60 µm. A mean circular profile of the vortex plates in Fig. 1a,b is shown in Fig. 1c. The surface profiles were measured with a Keyence VK-X1100 confocal laser scanning microscope using a 50× objective with $NA = 0.95$. The mean profiles indicate a smooth ramp with constant gradient and sharp height steps (discontinuities). For the vortex plate with $l = \pm 3$ (solid green line in Fig. 1c), the standard deviation of the height at the discontinuities is increased compared to the $l = \pm 1$ vortex plate (solid orange line in Fig. 1c). The cause for this can be seen in the detailed inset of Fig. 1b. The height steps do not coincide in the center of the vortex plate. Thus, when the profile is sampled from the center of the phase plate at varying radii r, the height steps shift steadily with increasing r. Away from the height steps, the standard deviation is 0.5 µm for both vortex plates, which matches the roughness of the manufacturing process. The total step height varies between the vortex plate for topological charge $l = \pm 1$ being 21.5 µm and for $l = \pm 3$ being only 18.3 µm on average. The remaining substrate thickness at the thinnest point of the vortex plate is 23 µm for the $l = \pm 1$ and 38 µm for the $l = \pm 3$ vortex plate. Nominally, for these heights an exact 2π phase shift is reached at photon energies of 8.0 keV and 6.8 keV, respectively. However, we used both vortex plates at a photon energy of 8.2 keV, as the aberration-corrected focusing optics

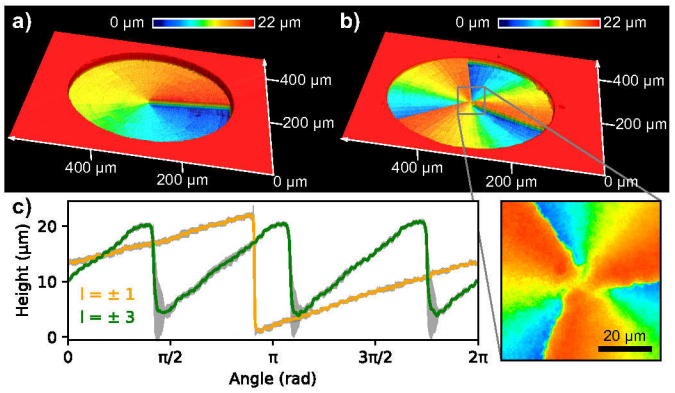


Fig. 1. Vortex phase plates manufactured by ultrashort-pulse laser ablation in fused silica. a) Phase plate with a step height of 21.5 µm to create a vortex with topological charge $l = \pm 1$ and a phase ramp of 2π at $E = 8.0$ keV. b) Phase plate with step height of 18.3 µm to create a vortex with topological charge $l = \pm 3$ and a phase ramp of 2π at $E = 6.8$ keV. The inset shows a detail of the central part. c) Height profile of the manufactured fused silica vortex plates shown in (a) and (b). The radial profile was sampled at radii r from $20\,\mu\text{m} \leq r \leq 150\,\mu\text{m}$ in 5 µm steps. The colored solid line shows the mean profile, the grey area represents the standard deviation. The outermost radius of both vortex plates is 200 µm.

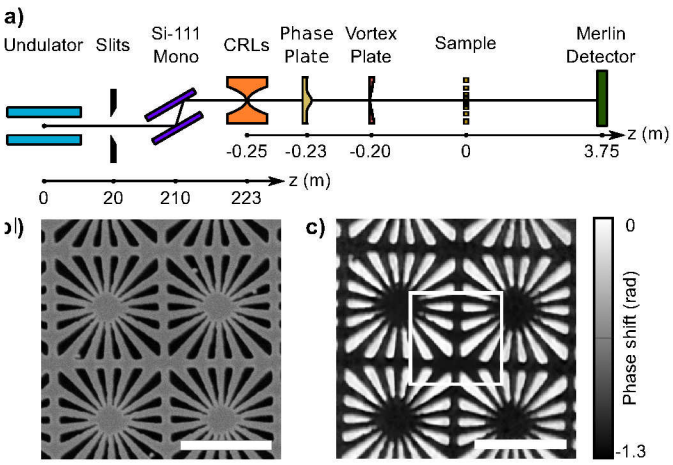


Fig. 2. a) Experimental setup at beamline I13-1 at DLS. A stack of Be-CRLs with a focal length $f = 250$ mm at $E = 8.2$ keV was used to focus the X-ray beam. An aberration-correcting phase plate was mounted approximately 10 mm after the lens exit to reduce spherical aberrations of the lenses. The vortex plates (cf. Fig. 1) were placed roughly 40 mm behind the lens exit to create a phase singularity. b) Scanning electron microscope image of the nanostructured tungsten layer on top of a diamond substrate layer, forming an array of Siemens stars with 50 nm smallest features. c) Ptychographically reconstructed object phase shift of the Siemens star test sample. The white square denotes the scanned area. Scale bars in b and c represent 2 µm. The shown regions in b and c do not coincide.

were optimized for that energy. The vortex plates can be used to either create a vortex with positive or negative topological charge by simply flipping them.

We verified the performance of the vortex plates by creating vortex beams at beamline I13-1 of Diamond Light Source (DLS) [16]. A sketch of the experimental setup is shown in Fig. 2a. We used a stack of 20 beryllium compound refractive lenses (Be CRLs) with an aperture of 300 µm and radius of curvature 50 µm, resulting in a 22 mm thick lens stack, to focus the beam [17]. At $E = 8.2$ keV the resulting focal length is 250 mm, reaching a NA of 0.49×10^{-3}. To increase the horizontal coherence length we created a secondary source using a pair of slits that was closed to 50 µm at a distance of 203 m upstream from the experiment (cf. Fig. 2). The vertical source is located 210 m upstream of the experiment and has a size of 13 µm. Therefore, a lateral coherence length of 0.5 mm × 2.2 mm was reached at the focusing Be CRL, exceeding its geometrical aperture. The coherent beam was characterized via ptychography [18–21], a scanning coherent X-ray diffraction method that retrieves both the complex object and the illuminating complex wavefield at the sample position from a set of diffraction patterns. A strongly scattering Siemens star test sample, etched into 1 µm thick tungsten with 50 nm smallest features (cf. Fig. 2b), was placed in the vicinity of the focal plane within the depth of field. The focused X-ray beam was scanned across the sample in a grid fashion with 100 nm step size, covering an area of 2 µm × 2 µm, as indicated by the white square in the reconstructed object shown in Fig. 2c. In total 441 far-field diffraction patterns with a dwell time of 1 s each were recorded by a quad chip Merlin photon-counting pixel detector [22] with 55 µm pixel size at a distance of 3.75 m downstream of the sample. Diffraction patterns were cropped to 512 × 512 pixel around the optical axis. The reconstructed complex wavefield at the object plane was subsequently propagated to the focal plane using the Fresnel-Kirchhoff diffraction integral. Here, we defined the experimental focal plane as that with the peak intensity along the caustic.

As the employed Be CRLs show spherical aberration [23] that would spoil the quality of the vortex beam, we used a corrective phase plate out of fused silica [24] to correct for this. The manufacturing process is similar to the one for the vortex plates described above. The corrective phase plate was aligned 10 mm downstream of the exit of the Be CRL stack via the Ronchi test [25] and ptychography as detailed in [24]. Fig. 3a,d shows the complex wavefield and phase distribution in focus, respectively, for an aberration-corrected Be CRL stack without any vortex phase plate installed. The full width at half maximum beam size is 143 nm, matching the theoretical model calculations well (cf. Fig. 3g). Afterwards, we installed an additional vortex plate roughly 40 mm behind the lens stack (cf. Fig. 2). Alignment was performed via a scintillator-based high-resolution X-ray camera and consecutive beam characterization via ptychography, again using the Siemens star test sample (cf. Fig. 2b,c). Measured complex vortex beam wavefields in the focal plane with $l = -1$ and $l = -3$ are shown in Fig. 3b,c, respectively. The phase distribution in focus for $l = -1$ and $l = -3$ is depicted in Fig. 3e,f, respectively. In the case of $l = -1$ the donut shape is very symmetric with a homogeneous radial intensity distribution. For $l = -3$ the ring is more irregular, originating likely from manufacturing inaccuracies of the vortex plate. The phase distribution in focus for the $l = -3$ vortex plate, shown in Fig. 3f, clearly indicates that the higher-order vortex has decayed into three first-order vortices. This separation can also be seen in Fig. 3c in the central area, where the three vortices are separated by very low intensity lines that form in between the phase singularities. Although vortices with $|l| > 1$ tend to decay into

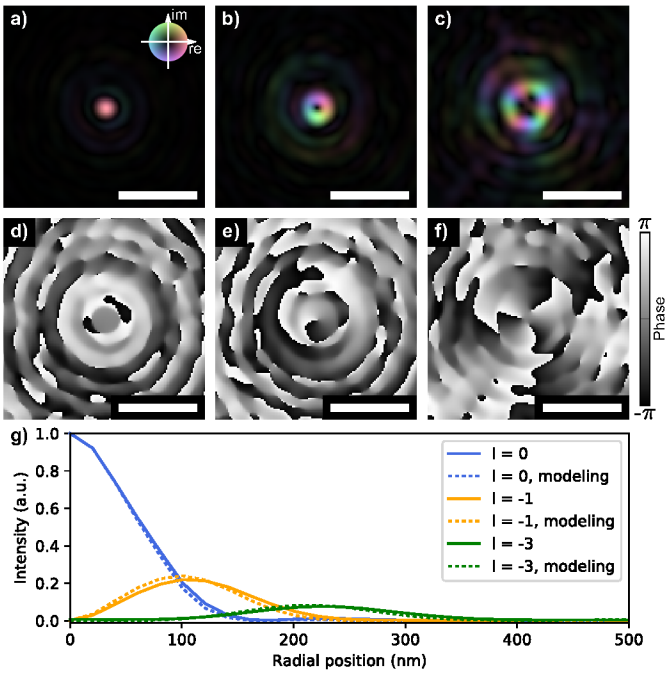


Fig. 3. Reconstructed wavefield (a, b, c) and phase (d, e, f) in focus for beams with topological charge $l = 0$ (a, d), $l = -1$ (b, e), and $l = -3$ (c, f). Scale bars in all images represent 1 µm. The high-order vortex in (c,f) has decayed into three first-order vortices. g) Radial intensity profile in focus achieved in the experiment compared to numerical modeling.

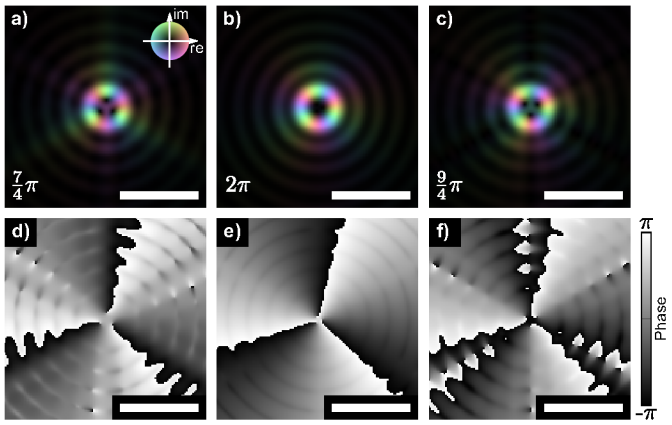


Fig. 4. Numerical model of the experiment with an ideally shaped $l = -3$ vortex plate to investigate the impact of fractional phase shifts. a, d) Numerically modeled focal spot and phase distribution for a vortex plate with $7/4\pi$ phase shift. b, e) Focal spot and phase for the ideal 2π phase shifting vortex plate. c, f) Simulated focal spot and phase for a $9/4\pi$ vortex plate. All scale bars represent 1 µm.

more stable $|l| = 1$ vortices due to aberrations and other experimental defects [26, 27], we believe the effect in this study to be dominated by the fractional 2π phase shift of the phase plate. Here, a thickness of 18.3 µm for the $l = -3$ vortex plate corresponds to 1.66π phase shift and results in a non-integer vortex beam [26, 28], as shown in Fig. 3c,f. When only considering the intensity distribution in focus, the radially integrated intensity depicted in Fig. 3g matches well with simulated phase plates with an appropriate 2π phase shift and fractional phase shifts seem to have a minor impact.

In Fig. 4 we have numerically modeled the experiment, but assume a perfect, aberration free lens and a perfectly manufactured vortex plate (with the same overall geometry as the fabricated one shown in Fig. 1b) with varying phase shifts around 2π. For the ideal 2π phase shifting case shown in Fig. 4b,e one observes no on-axis intensity in Fig. 4b, but the $l = -3$ vortex clearly has decayed into three $l = -1$ vortices with a distance of roughly 80 nm between them (cf. Fig. 4e). For the fractional 2π cases shown in Fig. 4a,d for $7/4\pi$ and in Fig. 4c,f for $9/4\pi$ phase shift, one clearly observes three intensity spokes originating from the optical axis (cf. Fig.4a,c). In addition the spacing between the three $l = -1$ vortices increased to approximately 160 nm. The intensities between the $l = -1$ vortices result from a compensation of the fractional 2π phase shift. Although the total angular momentum is still $l = -3$, the fractional phase shift leads to a non-zero transverse momentum with respect to the fixed optical axis, which gives an extrinsic contribution to the total orbital angular momentum [26].

In conclusion, we have demonstrated new capabilities to create hard X-ray vortex beams with moderate topological charges via refractive vortex phase plates that feature a smooth phase ramp. Being manufactured out of radiation hard fused silica might make them suitable for demanding high-intensity applications at X-ray free-electron laser and 4th generation diffraction-limited storage ring sources [29–34]. Similar ablation techniques are established for diamond [35] and potentially can be applied to backside ablation of single-crystal diamond substrates as well. Refractive phase plates present an alternative to forked gratings [9] and spiral zone plates [27], which eventually could also be fabricated out of diamond. Vortex plates potentially enable new experimental schemes, e. g., X-ray isochoric heating in a cylindrical geometry or investigation of magnetic structures [36, 37]. In combination with a split and delay line with collinear geometry [38] one could realize pump-probe schemes with and without a vortex plate, e. g., in the style of stimulated emission depletion microscopy [39]. In combination with high *NA* X-ray optics vortex beams could be used for the direct phasing of diffraction patterns from protein nanocrystals [40, 41] via ptychographic crystallography [42], dramatically reducing the amount of required data in time-resolved diffract-and-destroy experiments at XFELs. Another potential application is the manipulation or characterization of topologically complex matter like magnetic skyrmions through the exchange of OAM.

FUNDING.

F.S. acknowledges funding from the Volkswagen Foundation. Parts of this research were carried out at the coherence branch of beamline I13-1 at Diamond Light Source (DLS) within experiment MT17460-2.

REFERENCES

1. H. Rubinsztein-Dunlop, A. Forbes, M. V. Berry, M. R. Dennis, D. L. Andrews, M. Mansuripur, C. Denz, C. Alpmann, P. Banzer, T. Bauer, E. Karimi, L. Marrucci, M. Padgett, M. Ritsch-Marte, N. M. Litchinitser, N. P. Bigelow, C. Rosales-Guzmán, A. Belmonte, J. P. Torres, T. W. Neely, M. Baker, R. Gordon, A. B. Stilgoe, J. Romero, A. G. White, R. Fickler, A. E. Willner, G. Xie, B. McMorran, and A. M. Weiner, J. Opt. **19**, 013001 (2016).
2. H. He, M. E. J. Friese, N. R. Heckenberg, and H. Rubinsztein-Dunlop, Phys. Rev. Lett. **75**, 826 (1995).

3. M. Padgett and R. Bowman, Nat. Photonics **5**, 343 (2011).
4. J. Wang, J.-Y. Yang, I. M. Fazal, N. Ahmed, Y. Yan, H. Huang, Y. Ren, Y. Yue, S. Dolinar, M. Tur, and A. E. Willner, Nat. Photonics **6**, 488 (2012).
5. S. Fürhapter, A. Jesacher, S. Bernet, and M. Ritsch-Marte, Opt. Lett. **30**, 1953 (2005).
6. F. Tamburini, G. Anzolin, G. Umbriaco, A. Bianchini, and C. Barbieri, Phys. Rev. Lett. **97**, 163903 (2006).
7. A. G. Peele, P. J. McMahon, D. Paterson, C. Q. Tran, A. P. Mancuso, K. A. Nugent, J. P. Hayes, E. Harvey, B. Lai, and I. McNulty, Opt. Lett. **27**, 1752 (2002).
8. D. Cojoc, B. Kaulich, A. Carpentiero, S. Cabrini, L. Businaro, and E. D. Fabrizio, Microelectron. Eng. **83**, 1360 (2006). Micro- and Nano-Engineering MNE 2005.
9. J. C. T. Lee, S. J. Alexander, S. D. Kevan, S. Roy, and B. J. McMorran, Nat. Photonics **13**, 205 (2019).
10. C. David, S. Gorelick, S. Rutishauser, J. Krzywinski, J. Vila-Comamala, V. A. Guzenko, O. Bunk, E. Farm, M. Ritala, M. Cammarata, D. M. Fritz, R. Barrett, L. Samoylova, J. Grunert, and H. Sinn, Sci. Rep. **1**, 57 (2011).
11. F. Uhlén, D. Nilsson, A. Holmberg, H. M. Hertz, C. G. Schroer, F. Seiboth, J. Patommel, V. Meier, R. Hoppe, A. Schropp, H. J. Lee, B. Nagler, E. Galtier, J. Krzywinski, H. Sinn, and U. Vogt, Opt. Express **21**, 8051 (2013).
12. S. Sasaki and I. McNulty, Phys. Rev. Lett. **100**, 124801 (2008).
13. J. Bahrdt, K. Holldack, P. Kuske, R. Müller, M. Scheer, and P. Schmid, Phys. Rev. Lett. **111**, 034801 (2013).
14. E. Hemsing, A. Knyazik, M. Dunning, D. Xiang, A. Marinelli, C. Hast, and J. B. Rosenzweig, Nat. Phys. **9**, 549 (2013).
15. E. Hemsing and A. Marinelli, Phys. Rev. Lett. **109**, 224801 (2012).
16. C. Rau, U. Wagner, A. Peach, I. K. Robinson, B. Singh, G. Wilkin, and C. Jones, AIP Conf. Proc. **1234**, 121 (2010).
17. B. Lengeler, C. Schroer, J. Tummler, B. Benner, M. Richwin, A. Snigirev, I. Snigireva, and M. Drakopoulos, J. Synchrotron Radiat. **6**, 1153 (1999).
18. A. Schropp, P. Boye, J. M. Feldkamp, R. Hoppe, J. Patommel, D. Samberg, S. Stephan, K. Giewekemeyer, R. N. Wilke, T. Salditt, J. Gulden, A. P. Mancuso, I. A. Vartanyants, E. Weckert, S. Schoder, M. Burghammer, and C. G. Schroer, Appl. Phys. Lett. **96**, 091102 (2010).
19. C. M. Kewish, M. Guizar-Sicairos, C. Liu, J. Qian, B. Shi, C. Benson, A. M. Khounsary, J. Vila-Comamala, O. Bunk, J. R. Fienup, A. T. Macrander, and L. Assoufid, Opt. Express **18**, 23420 (2010).
20. S. Hönig, R. Hoppe, J. Patommel, A. Schropp, S. Stephan, S. Schöder, M. Burghammer, and C. G. Schroer, Opt. Express **19**, 16324 (2011).
21. A. Schropp, R. Hoppe, V. Meier, J. Patommel, F. Seiboth, H. J. Lee, B. Nagler, E. C. Galtier, B. Arnold, U. Zastrau, J. B. Hastings, D. Nilsson, F. Uhlén, U. Vogt, H. M. Hertz, and C. G. Schroer, Sci. Rep. **3**, 01633 (2013).
22. R. Plackett, I. Horswell, E. N. Gimenez, J. Marchal, D. Omar, and N. Tartoni, J. Instrumentation **8**, C01038 (2013).
23. F. Seiboth, F. Wittwer, M. Scholz, M. Kahnt, M. Seyrich, A. Schropp, U. Wagner, C. Rau, J. Garrevoet, G. Falkenberg, and C. G. Schroer, J. Synchrotron Radiat. **25**, 108 (2018).
24. F. Seiboth, A. Schropp, M. Scholz, F. Wittwer, C. Rödel, M. Wünsche, T. Ullsperger, S. Nolte, J. Rahomäki, K. Parfeniukas, S. Giakoumidis, U. Vogt, U. Wagner, C. Rau, U. Boesenberg, J. Garrevoet, G. Falkenberg, E. C. Galtier, H. J. Lee, B. Nagler, and C. G. Schroer, Nat. Commun. **8**, 14623 (2017).
25. F. Uhlén, J. Rahomäki, D. Nilsson, F. Seiboth, C. Sanz, U. Wagner, C. Rau, C. G. Schroer, and U. Vogt, J. Synchrotron Radiat. **21**, 1105 (2014).
26. J. Leach, E. Yao, and M. J. Padgett, New J. Phys. **6**, 71 (2004).
27. J. Vila-Comamala, A. Sakdinawat, and M. Guizar-Sicairos, Opt. Lett. **39**, 5281 (2014).
28. M. V. Berry, J. Opt. A: Pure Appl. Opt. **6**, 259 (2004).
29. C. Bostedt, S. Boutet, D. M. Fritz, Z. Huang, H. J. Lee, H. T. Lemke, A. Robert, W. F. Schlotter, J. J. Turner, and G. J. Williams, Rev. Mod. Phys. **88**, 015007 (2016).
30. T. Ishikawa, H. Aoyagi, T. Asaka, Y. Asano, N. Azumi, T. Bizen, H. Ego, K. Fukami, T. Fukui, Y. Furukawa, S. Goto, H. Hanaki, T. Hara, T. Hasegawa, T. Hatsui, A. Higashiya, T. Hirono, N. Hosoda, M. Ishii, T. Inagaki, Y. Inubushi, T. Itoga, Y. Joti, M. Kago, T. Kameshima, H. Kimura, Y. Kirihara, A. Kiyomichi, T. Kobayashi, C. Kondo, T. Kudo, H. Maesaka, X. M. Marechal, T. Masuda, S. Matsubara, T. Matsumoto, T. Matsushita, S. Matsui, M. Nagasono, N. Nariyama, H. Ohashi, T. Ohata, T. Ohshima, S. Ono, Y. Otake, C. Saji, T. Sakurai, T. Sato, K. Sawada, T. Seike, K. Shirasawa, T. Sugimoto, S. Suzuki, S. Takahashi, H. Takebe, K. Takeshita, K. Tamasaku, H. Tanaka, R. Tanaka, T. Tanaka, T. Togashi, K. Togawa, A. Tokuhisa, H. Tomizawa, K. Tono, S. Wu, M. Yabashi, M. Yamaga, A. Yamashita, K. Yanagida, C. Zhang, T. Shintake, H. Kitamura, and N. Kumagai, Nat Photon **6**, 540 (2012).
31. M. Altarelli, Nucl. Instruments Methods Phys. Res. Sect. B: Beam Interactions with Mater. Atoms **269**, 2845 (2011).
32. P. F. Tavares, E. Al-Dmour, Å. Andersson, F. Cullinan, B. N. Jensen, D. Olsson, D. K. Olsson, M. Sjöström, H. Tarawneh, S. Thorin, and A. Vorozhtsov, J. Synchrotron Radiat. **25**, 1291 (2018).
33. P. Raimondi, Synchrotron Radiat. News **29**, 8 (2016).
34. C. G. Schroer, I. Agapov, W. Brefeld, R. Brinkmann, Y.-C. Chae, H.-C. Chao, M. Eriksson, J. Keil, X. Nuel Gavaldà, R. Röhlsberger, O. H. Seeck, M. Sprung, M. Tischer, R. Wanzenberg, and E. Weckert, J. Synchrotron Radiat. **25**, 1277 (2018).
35. V. Konov, Laser & Photonics Rev. **6**, 739 (2012).
36. M. van Veenendaal and I. McNulty, Phys. Rev. Lett. **98**, 157401 (2007).
37. M. van Veenendaal, Phys. Rev. B **92**, 245116 (2015).
38. W. Roseker, S. Lee, M. Walther, H. Schulte-Schrepping, H. Franz, A. Gray, M. Sikorski, P. H. Fuoss, G. B. Stephenson, A. Robert, and G. Grübel, ProcSPIE **8504**, 85040I (2012).
39. S. W. Hell and J. Wichmann, Opt. Lett. **19**, 780 (1994).
40. J. C. H. Spence, N. A. Zatsepin, and C. Li, Philos. Transactions Royal Soc. B: Biol. Sci. **369**, 20130325 (2014).
41. D. Jüstel, G. Friesecke, and R. D. James, Acta Crystallogr. Sect. A: Foundations Adv. **72**, 190 (2016).
42. P. D. Nellist and J. M. Rodenburg, Acta Crystallogr. Sect. A **54**, 49 (1998).

FULL REFERENCES

1. H. Rubinsztein-Dunlop, A. Forbes, M. V. Berry, M. R. Dennis, D. L. Andrews, M. Mansuripur, C. Denz, C. Alpmann, P. Banzer, T. Bauer, E. Karimi, L. Marrucci, M. Padgett, M. Ritsch-Marte, N. M. Litchinitser, N. P. Bigelow, C. Rosales-Guzmán, A. Belmonte, J. P. Torres, T. W. Neely, M. Baker, R. Gordon, A. B. Stilgoe, J. Romero, A. G. White, R. Fickler, A. E. Willner, G. Xie, B. McMorran, and A. M. Weiner, "Roadmap on structured light," J. Opt. **19**, 013001 (2016).
2. H. He, M. E. J. Friese, N. R. Heckenberg, and H. Rubinsztein-Dunlop, "Direct observation of transfer of angular momentum to absorptive particles from a laser beam with a phase singularity," Phys. Rev. Lett. **75**, 826–829 (1995).
3. M. Padgett and R. Bowman, "Tweezers with a twist," Nat. Photonics **5**, 343–348 (2011).
4. J. Wang, J.-Y. Yang, I. M. Fazal, N. Ahmed, Y. Yan, H. Huang, Y. Ren, Y. Yue, S. Dolinar, M. Tur, and A. E. Willner, "Terabit free-space data transmission employing orbital angular momentum multiplexing," Nat. Photonics **6**, 488–496 (2012).
5. S. Fürhapter, A. Jesacher, S. Bernet, and M. Ritsch-Marte, "Spiral interferometry," Opt. Lett. **30**, 1953–1955 (2005).
6. F. Tamburini, G. Anzolin, G. Umbriaco, A. Bianchini, and C. Barbieri, "Overcoming the rayleigh criterion limit with optical vortices," Phys. Rev. Lett. **97**, 163903 (2006).
7. A. G. Peele, P. J. McMahon, D. Paterson, C. Q. Tran, A. P. Mancuso, K. A. Nugent, J. P. Hayes, E. Harvey, B. Lai, and I. McNulty, "Observation of an x-ray vortex," Opt. Lett. **27**, 1752–1754 (2002).
8. D. Cojoc, B. Kaulich, A. Carpentiero, S. Cabrini, L. Businaro, and E. D. Fabrizio, "X-ray vortices with high topological charge," Microelectron. Eng. **83**, 1360–1363 (2006). Micro- and Nano-Engineering MNE 2005.
9. J. C. T. Lee, S. J. Alexander, S. D. Kevan, S. Roy, and B. J. McMorran, "Laguerre-gauss and hermite-gauss soft x-ray states generated using diffractive optics," Nat. Photonics **13**, 205—209 (2019).
10. C. David, S. Gorelick, S. Rutishauser, J. Krzywinski, J. Vila-Comamala, V. A. Guzenko, O. Bunk, E. Farm, M. Ritala, M. Cammarata, D. M. Fritz, R. Barrett, L. Samoylova, J. Grunert, and H. Sinn, "Nanofocusing of hard X-ray free electron laser pulses using diamond based Fresnel zone plates," Sci. Rep. **1**, 57 (2011).
11. F. Uhlén, D. Nilsson, A. Holmberg, H. M. Hertz, C. G. Schroer, F. Seiboth, J. Patommel, V. Meier, R. Hoppe, A. Schropp, H. J. Lee, B. Nagler, E. Galtier, J. Krzywinski, H. Sinn, and U. Vogt, "Damage investigation on tungsten and diamond diffractive optics at a hard x-ray free-electron laser," Opt. Express **21**, 8051–8061 (2013).
12. S. Sasaki and I. McNulty, "Proposal for generating brilliant x-ray beams carrying orbital angular momentum," Phys. Rev. Lett. **100**, 124801 (2008).
13. J. Bahrdt, K. Holldack, P. Kuske, R. Müller, M. Scheer, and P. Schmid, "First observation of photons carrying orbital angular momentum in undulator radiation," Phys. Rev. Lett. **111**, 034801 (2013).
14. E. Hemsing, A. Knyazik, M. Dunning, D. Xiang, A. Marinelli, C. Hast, and J. B. Rosenzweig, "Coherent optical vortices from relativistic electron beams," Nat. Phys. **9**, 549–553 (2013).
15. E. Hemsing and A. Marinelli, "Echo-enabled x-ray vortex generation," Phys. Rev. Lett. **109**, 224801 (2012).
16. C. Rau, U. Wagner, A. Peach, I. K. Robinson, B. Singh, G. Wilkin, and C. Jones, "The diamond beamline i13l for imaging and coherence," AIP Conf. Proc. **1234**, 121–125 (2010).
17. B. Lengeler, C. Schroer, J. Tummler, B. Benner, M. Richwin, A. Snigirev, I. Snigireva, and M. Drakopoulos, "Imaging by parabolic refractive lenses in the hard x-ray range," J. Synchrotron Radiat. **6**, 1153–1167 (1999).
18. A. Schropp, P. Boye, J. M. Feldkamp, R. Hoppe, J. Patommel, D. Samberg, S. Stephan, K. Giewekemeyer, R. N. Wilke, T. Salditt, J. Gulden, A. P. Mancuso, I. A. Vartanyants, E. Weckert, S. Schoder, M. Burghammer, and C. G. Schroer, "Hard x-ray nanobeam characterization by coherent diffraction microscopy," Appl. Phys. Lett. **96**, 091102 (2010).
19. C. M. Kewish, M. Guizar-Sicairos, C. Liu, J. Qian, B. Shi, C. Benson, A. M. Khounsary, J. Vila-Comamala, O. Bunk, J. R. Fienup, A. T. Macrander, and L. Assoufid, "Reconstruction of an astigmatic hard X-ray beam and alignment of K-B mirrors from ptychographic coherent diffraction data," Opt. Express **18**, 23420–23427 (2010).
20. S. Hönig, R. Hoppe, J. Patommel, A. Schropp, S. Stephan, S. Schöder, M. Burghammer, and C. G. Schroer, "Full optical characterization of coherent x-ray nanobeams by ptychographic imaging," Opt. Express **19**, 16324–16329 (2011).
21. A. Schropp, R. Hoppe, V. Meier, J. Patommel, F. Seiboth, H. J. Lee, B. Nagler, E. C. Galtier, B. Arnold, U. Zastrau, J. B. Hastings, D. Nilsson, F. Uhlén, U. Vogt, H. M. Hertz, and C. G. Schroer, "Full spatial characterization of a nanofocused x-ray free-electron laser beam by ptychographic imaging," Sci. Rep. **3**, 01633 (2013).
22. R. Plackett, I. Horswell, E. N. Gimenez, J. Marchal, D. Omar, and N. Tartoni, "Merlin: a fast versatile readout system for medipix3," J. Instrumentation **8**, C01038 (2013).
23. F. Seiboth, F. Wittwer, M. Scholz, M. Kahnt, M. Seyrich, A. Schropp, U. Wagner, C. Rau, J. Garrevoet, G. Falkenberg, and C. G. Schroer, "Nanofocusing with aberration-corrected rotationally parabolic refractive x-ray lenses," J. Synchrotron Radiat. **25**, 108–115 (2018).
24. F. Seiboth, A. Schropp, M. Scholz, F. Wittwer, C. Rödel, M. Wünsche, T. Ullsperger, S. Nolte, J. Rahomäki, K. Parfeniukas, S. Giakoumidis, U. Vogt, U. Wagner, C. Rau, U. Boesenberg, J. Garrevoet, G. Falkenberg, E. C. Galtier, H. J. Lee, B. Nagler, and C. G. Schroer, "Perfect x-ray focusing via fitting corrective glasses to aberrated optics," Nat. Commun. **8**, 14623 (2017).
25. F. Uhlén, J. Rahomäki, D. Nilsson, F. Seiboth, C. Sanz, U. Wagner, C. Rau, C. G. Schroer, and U. Vogt, "Ronchi test for characterization of X-ray nanofocusing optics and beamlines," J. Synchrotron Radiat. **21**, 1105–1109 (2014).
26. J. Leach, E. Yao, and M. J. Padgett, "Observation of the vortex structure of a non-integer vortex beam," New J. Phys. **6**, 71–71 (2004).
27. J. Vila-Comamala, A. Sakdinawat, and M. Guizar-Sicairos, "Characterization of x-ray phase vortices by ptychographic coherent diffractive imaging," Opt. Lett. **39**, 5281–5284 (2014).
28. M. V. Berry, "Optical vortices evolving from helicoidal integer and fractional phase steps," J. Opt. A: Pure Appl. Opt. **6**, 259–268 (2004).
29. C. Bostedt, S. Boutet, D. M. Fritz, Z. Huang, H. J. Lee, H. T. Lemke, A. Robert, W. F. Schlotter, J. J. Turner, and G. J. Williams, "Linac coherent light source: The first five years," Rev. Mod. Phys. **88**, 015007 (2016).
30. T. Ishikawa, H. Aoyagi, T. Asaka, Y. Asano, N. Azumi, T. Bizen, H. Ego, K. Fukami, T. Fukui, Y. Furukawa, S. Goto, H. Hanaki, T. Hara, T. Hasegawa, T. Hatsui, A. Higashiya, T. Hirono, N. Hosoda, M. Ishii, T. Inagaki, Y. Inubushi, T. Itoga, Y. Joti, M. Kago, T. Kameshima, H. Kimura, Y. Kirihara, A. Kiyomichi, T. Kobayashi, C. Kondo, T. Kudo, H. Maesaka, X. M. Marechal, T. Masuda, S. Matsubara, T. Matsumoto, T. Matsushita, S. Matsui, M. Nagasono, N. Nariyama, H. Ohashi, T. Ohata, T. Ohshima, S. Ono, Y. Otake, C. Saji, T. Sakurai, T. Sato, K. Sawada, T. Seike, K. Shirasawa, T. Sugimoto, S. Suzuki, S. Takahashi, H. Takebe, K. Takeshita, K. Tamasaku, H. Tanaka, R. Tanaka, T. Tanaka, T. Togashi, K. Togawa, A. Tokuhisa, H. Tomizawa, K. Tono, S. Wu, M. Yabashi, M. Yamaga, A. Yamashita, K. Yanagida, C. Zhang, T. Shintake, H. Kitamura, and N. Kumagai, "A compact x-ray free-electron laser emitting in the sub-angstrom region," Nat Photon **6**, 540–544 (2012).
31. M. Altarelli, "The european x-ray free-electron laser facility in hamburg," Nucl. Instruments Methods Phys. Res. Sect. B: Beam Interactions with Mater. Atoms **269**, 2845–2849 (2011).
32. P. F. Tavares, E. Al-Dmour, Å. Andersson, F. Cullinan, B. N. Jensen, D. Olsson, D. K. Olsson, M. Sjöström, H. Tarawneh, S. Thorin, and A. Vorozhtsov, "Commissioning and first-year operational results of the MAXIV 3GeV ring," J. Synchrotron Radiat. **25**, 1291–1316 (2018).
33. P. Raimondi, "Esrf-ebs: The extremely brilliant source project," Synchrotron Radiat. News **29**, 8–15 (2016).
34. C. G. Schroer, I. Agapov, W. Brefeld, R. Brinkmann, Y.-C. Chae, H.-C. Chao, M. Eriksson, J. Keil, X. Nuel Gavaldà, R. Röhlsberger, O. H. Seeck, M. Sprung, M. Tischer, R. Wanzenberg, and E. Weckert, "PETRA IV: the ultralow-emittance source project at DESY," J. Synchrotron Radiat. **25**, 1277–1290 (2018).

35. V. Konov, "Laser in micro and nanoprocessing of diamond materials," Laser & Photonics Rev. **6**, 739–766 (2012).
36. M. van Veenendaal and I. McNulty, "Prediction of strong dichroism induced by x rays carrying orbital momentum," Phys. Rev. Lett. **98**, 157401 (2007).
37. M. van Veenendaal, "Interaction between x-ray and magnetic vortices," Phys. Rev. B **92**, 245116 (2015).
38. W. Roseker, S. Lee, M. Walther, H. Schulte-Schrepping, H. Franz, A. Gray, M. Sikorski, P. H. Fuoss, G. B. Stephenson, A. Robert, and G. Grübel, "Hard x-ray delay line for x-ray photon correlation spectroscopy and jitter-free pump-probe experiments at lcls," ProcSPIE **8504**, 85040I (2012).
39. S. W. Hell and J. Wichmann, "Breaking the diffraction resolution limit by stimulated emission: stimulated-emission-depletion fluorescence microscopy," Opt. Lett. **19**, 780–782 (1994).
40. J. C. H. Spence, N. A. Zatsepin, and C. Li, "Coherent convergent-beam time-resolved x-ray diffraction," Philos. Transactions Royal Soc. B: Biol. Sci. **369**, 20130325 (2014).
41. D. Jüstel, G. Friesecke, and R. D. James, "Bragg–von laue diffraction generalized to twisted x-rays," Acta Crystallogr. Sect. A: Foundations Adv. **72**, 190–196 (2016).
42. P. D. Nellist and J. M. Rodenburg, "Electron Ptychography. I. Experimental Demonstration Beyond the Conventional Resolution Limits," Acta Crystallogr. Sect. A **54**, 49–60 (1998).